Supplementary Information

Multi-dentate, Weakly Coordinating Co-solvents Enabling Balanced Ion Dissociation/Desolvation Kinetics for Cryogenic Lithium Metal Batteries

Yihuan Zhou[a], Haoqing Ji[a,*], Yiwei Zheng[a,b,*], Diankuan Gu[a], Yining Ran[a], Qihang Jia[a], Mengfan Wang[a], Tao Qian[c], Xiaoping Wang[d], Chenglin Yan[a,e,*]

[a] *Collaborative Innovation Center of Suzhou Nano Science and Technology, College of Energy Soochow University, Suzhou 215006, China*

[b] *School of Material Science & Engineering, University of Jinan, Jinan 250022, China*

[c] *College of Chemistry and Chemical Engineering, Nantong University, Seyuan 9, Nantong 226019, China*

[d] *Beijing Comens New Materials Co., Ltd, Beijing 102502, China*

[e] *School of Petrochemical Engineering, Changzhou University, Changzhou 213164, China*

E-mails: jhq18@suda.edu.cn (H. Ji); mse_zhengyw@ujn.edu.cn (Y. Zheng); c.yan@suda.edu.cn (C. Yan).

1. Experimental section

1.1 Materials

Trimethoxymethane (TMM, >98.0%) was purchased from TCI, while 1,3-dioxolane (DOL, 99.9%), lithium bis(fluorosulfonyl)imide (LiFSI, 99.9%), and lithium nitrate ($LiNO_3$, 99.9%) were obtained from DoDoChem. Li foil with the thickness of 450 μm was supplied by Guangdong Canrd New Energy Technology Co., Ltd. Copper foil (9 μm thick), Celgard 2500 separators, and 2025-type coin cell cases were purchased from Shenzhen MTI. Both the Cu foil and separator were punched into discs of 14 mm diameter prior to use.

1.2 Electrode preparation.

$LiNi_{0.8}Co_{0.1}Mn_{0.1}O_2$ (NCM811) cathodes were prepared by mixing 80 wt% NCM811, 10 wt% conductive carbon (Super-P), and 10 wt% polyvinylidene fluoride (PVDF) in NMP solvent. The resultant slurry was coated onto Al foil current collector (single side) and transferred into a vacuum oven for drying at 80 °C overnight. Then the obtained NCM811 electrode was punched into circular disks (12 mm in diameter) for assembly into half cells.

1.3 Electrolyte preparation.

All electrolytes were prepared in an argon-filled glovebox with H_2O < 0.1 ppm and O_2 < 0.1 ppm. TMM was dried by molecular sieve (4 Å) before use. First, 1.5 mmol LiFSI was added to 1 mL a series of mixed solutions of TMM and DOL (with TMM: DOL volume ratios of 10:0, 7:3, 5:5, and 3:7). The resulting mixtures were then stirred for 12 h to obtain the corresponding electrolytes, denoted as TMM, TD73, TD55, and TD37, respectively.

1.4 Electrochemical measurements.

All cells were assembled in an argon-filled glovebox with H_2O < 0.1 ppm and O_2 < 0.1 ppm. The charging-discharging tests were performed on a Land battery testing system (Wuhan Land electronics Co. Ltd., China). NCM811||Li coin cells were assembled in 2025-type aluminum-coated coin cells in the glove box, using Li foil (450 μm) as the anode, a polypropylene (Celgard 2500) separator, and 60 μL of electrolyte. The test protocol for Li||NCM811 coin cells was that 0.1C

charging and 0.1C discharging at a voltage range of 3-4.2 V from 25 °C to −40 °C. Low-temperature charge-discharge curves of the Li||NCM811 cells were obtained from the second cycle at the corresponding temperature. Li||Cu cells were assembled with Cu as the working electrode and Li foil as the counter/reference electrode. Symmetric Li||Li cells were assembled using two Li metal electrodes. The Li plating/stripping coulombic efficiency (CE) was evaluated in Li/Cu half cells following the Aurbach measurement protocol.[1] Li plating capacity Q_P was pre-deposited at a current density of 0.5 mA cm^{-2} and a capacity of 5 mAh cm^{-2}. Then, Li metal was plating/stripping for 10 (n) cycles at a fixed capacity (Q_C = 0.5 mAh cm^{-2}). Finally, a capacity retention (Q_R) was measured by a final Li stripping process at 0.5 mA cm^{-2}. The CE value can be calculated by the following equation:

$$CE = \frac{nQ_c + Q_r}{nQ_c + Q_p}$$

Li||Li symmetric cells were cycled at (1 mA cm^{-2}, 1 mAh cm^{-2}) or (0.5 mA cm^{-2} and 0.5 mAh cm^{-2}). Li||Cu half cells were cycled at (0.5 mA cm^{-2} and 0.5 mAh cm^{-2}) at 25 and −20 °C, while cycled at (0.2 mA cm^{-2} and 0.2 mAh cm^{-2}) at -40 °C. The activation energy (Ea) was determined by fitting the data to the Arrhenius equation below:

$$\frac{1}{R_{ct}} = Ae^{-\frac{E_a}{RT}}$$

where R represents the impedance of charge transfer process, A is the pre-exponential factor, E_a is the molar activation energy, R is the universal gas constant, and T is the absolute temperature.

For Linear sweep voltammetry (LSV) test, Li||Al cells were assembled of thick Li metal anode, separator, and Al foil with a sweep rate of 1 mV s^{-1}. In situ electrochemical impedance spectroscopy (EIS) test in the frequency range from 0.1 Hz-100 kHz.: The NCM811||Li battery within the in situ EIS characterization was tested at 0.2 C and a voltage window of 3.0-4.2 V at −20 °C. The distribution of relaxation time (DRT) was obtained by transforming the EIS data using an open-source MATLAB code.[2]

Ionic conductivity of the bulk electrolytes was directly measured on a METTLER TOLEDO Seven Excellence S700-B at different temperatures.

1.5 Materials characterizations.

Scanning electron microscopy (SEM) was performed using a field-emission SEM (SU8010, Hitachi, Japan). Li metal samples for SEM analysis were harvested from cycled coin cells within an argon-filled glove box. Before imaging, the samples were rinsed with dimethyl carbonate (DMC) and subsequently dried inside the glove box. To prevent air exposure, the dried samples were transferred to the SEM specimen chamber using a sealed transfer vessel. Coaxial nuclear magnetic resonance (NMR) spectroscopy was conducted with a Bruker Avance NEO 400 MHz at 25 °C. The NMR tube was loaded with the electrolyte mixture, while a 1 M solution of LiCl in deuterium oxide (D2O), serving as the internal standard, was isolated from the main electrolyte volume within the tube using a capillary separator. X-ray photoelectron spectroscopy (XPS) measurements were carried out in an ultrahigh vacuum Escalab 25 0Xi (Thermo Fisher) setup equipped with a monochromatic Al Ka X-ray source (1486.6 eV; anode operating at 15 kV and 20 mA). To ensure accurate calibration of the Ar^+ etching rate, we used the standard testing parameters (Sample: Tb_2O_5, etching rate is 0.21 nm/s) provided by the Thermo Fisher Scientific. The Fourier Transform infrared (FTIR) spectroscopy measurement was conducted with a Thermo Scientific Nicolet iS20 FTIR spectrometer. The Raman spectra were recorded on a Lab RAMHR confocal Raman system with 532 nm diode laser excitation at room temperature.

2. Computational section

2.1 DFT calculations

All geometry optimizations and electronic-structure calculations for the target molecules and solvation clusters were performed using Gaussian 16. Calculations were carried out at the B3LYP-D3(BJ)/6-311+G(d,p) level of theory. Electronic-structure analyses and post-processing were conducted using Multiwfn 3.8(dev),[3] including extraction of HOMO/LUMO energies and evaluation of desolvation energies for representative solvation structures. Molecular electrostatic potential (ESP) mapped surfaces were generated based on the computed ESP and visualized using VMD 1.9.3.[4] The desolvation energy of a solvent molecule X from a given solvation structure (SS) was defined as the energy required to remove one molecule X from SS to form SS–X:

$E_{desolv}=E(SS-X)+E(X)-E(SS)$, where E denotes the electronic energy obtained from the corresponding DFT calculations.

2.2 Molecular dynamics simulations and solvation analysis

Molecular dynamics (MD) simulations were performed for three electrolyte systems at both 298.15 K and 233.15 K. The three systems correspond to neat TMM, the TD73 electrolyte, and the TDN electrolyte, respectively. Specifically, the TMM system consisted of 150 Li^+, 150 FSI^-, and 914 TMM molecules. The TD73 system contained 150 Li^+, 150 FSI^-, 640 TMM, and 429 DOL molecules. The TDN system comprised 160 Li^+, 150 FSI^-, 10 NO_3^-, 640 TMM, and 429 DOL molecules. Lithium ions were described using default Amber parameters, while all other species were modeled using the GAFF2 force field.[5] Atomic partial charges were derived by Multiwfn (version 3.8-dev) using the RESP scheme[6] based on electrostatic potentials calculated at the B3LYP-D3(BJ)/6-311+G(d,p) level of theory in Gaussian 16 program. A charge scaling factor of 0.8 was employed for ions to account for electronic polarization effects.[7] Prior to production runs, each system was subjected to energy minimization to remove unfavorable contacts. Subsequently, MD simulations were carried out under constant temperature (298.15 K or 233.15 K, with V-rescale thermostat) and pressure (1 bar, with Berendsen barostat) conditions for 50 ns with a time step of 1 fs. A nonbonded interaction cutoff of 1.2 nm was applied. Trajectories were saved every 10 ps for subsequent structural and dynamical analyses. Trajectory analyses for solvation-species classification and residence-time evaluation were performed using in-house codes. A solvent molecule or an anion was considered to belong to the Li^+ solvation sheath when any oxygen atom within that species was located within 3.0 Å of a Li^+ ion. For residence-time analysis, the last 40 ns of each 50 ns trajectory were analyzed. The solvation environment of each Li^+ ion was tracked frame-by-frame, and a solvent (or anion) was defined as "resident" only if it continuously remained within the same Li^+ solvation sheath according to the above distance criterion. This approach enables quantitative comparison of solvation-structure persistence and exchange dynamics across different electrolyte compositions and temperatures.

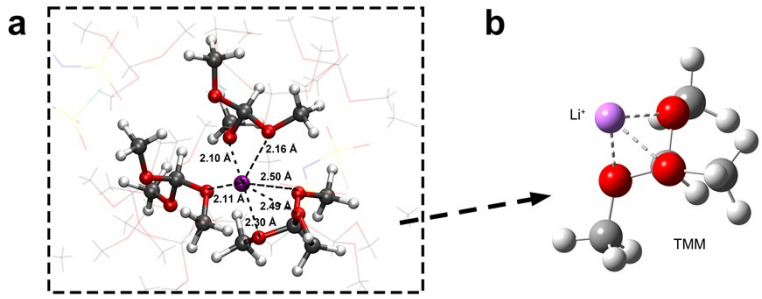

Fig. S1 (a) The representative Li^+ solvation structure extracted from the MD simulations of TMM electrolyte. (b) Optimized coordination structures of TMM-Li^+ by DFT.

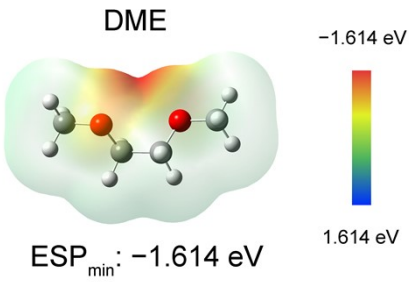

Fig. S2 ESP maps and corresponding ESP_{min} values for DME.

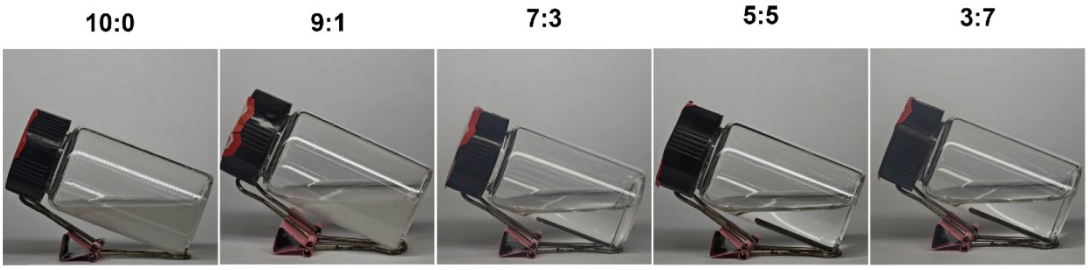

Fig. S3 The solubility data of 0.1M $LiNO_3$ in electrolytes with different volume ratios of TMM to DOL

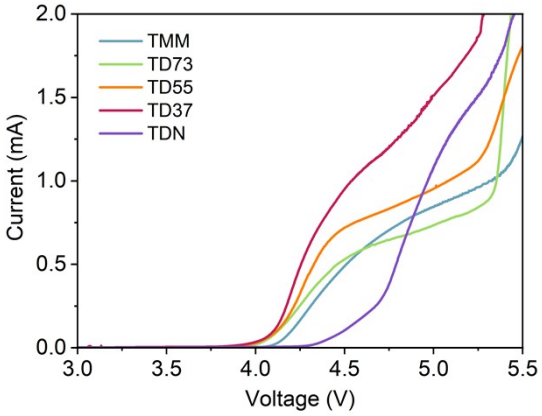

Fig. S4 Oxidation stability of different electrolytes in Li||Al half cells evaluated by LSV.

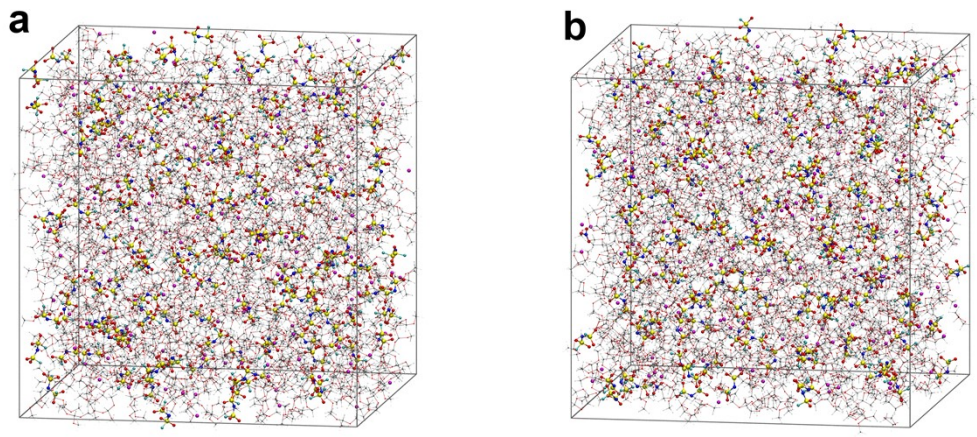

Fig. S5 Molecular dynamics simulations snapshots at 25 °C for (a)TMM and (b) TDN electrolytes.

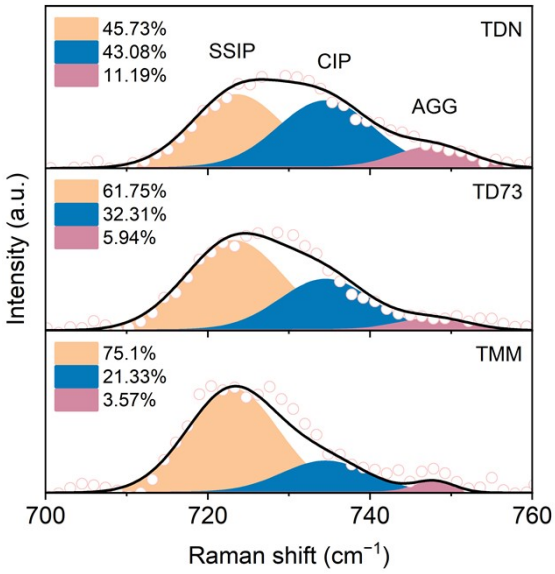

Fig. S6 Raman spectra of TMM, TD73, and TDN electrolytes.

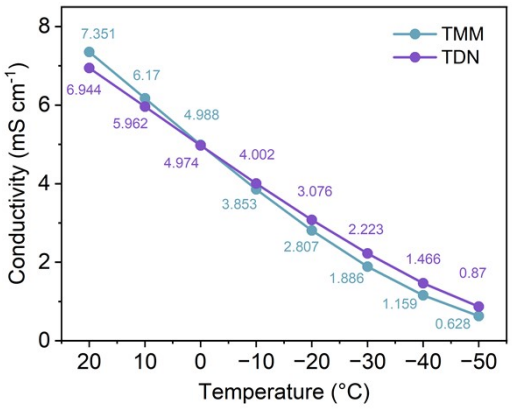

Fig. S7 The conductivities of the TMM and TDN electrolytes at different temperature.

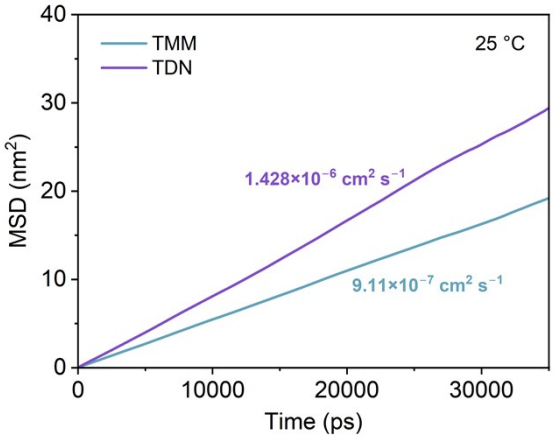

Fig. S8 Li^+ diffusion coefficients of the TMM and TDN electrolytes at 25 °C.

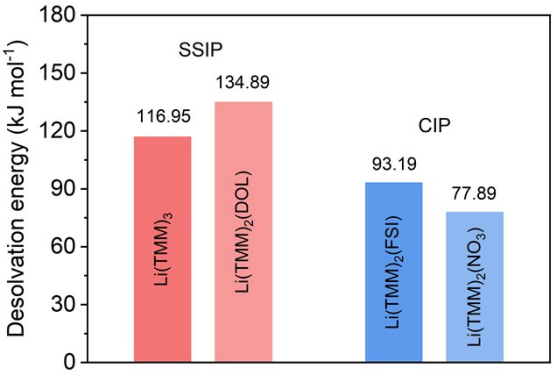

Fig. S9 The binding energy between Li^+ and TMM molecules in different solvation clusters.

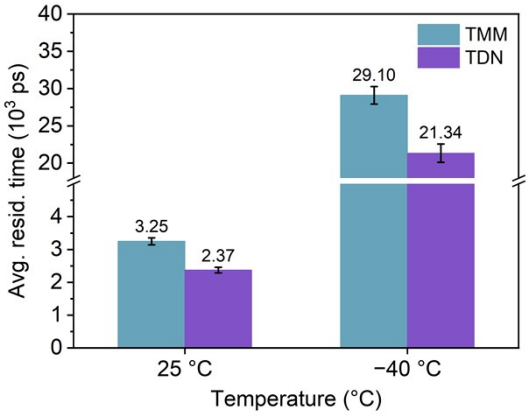

Fig. S10 The average residence time of TMM molecules in the Li^+ solvation sheath in different electrolytes at 25 °C and −40 °C

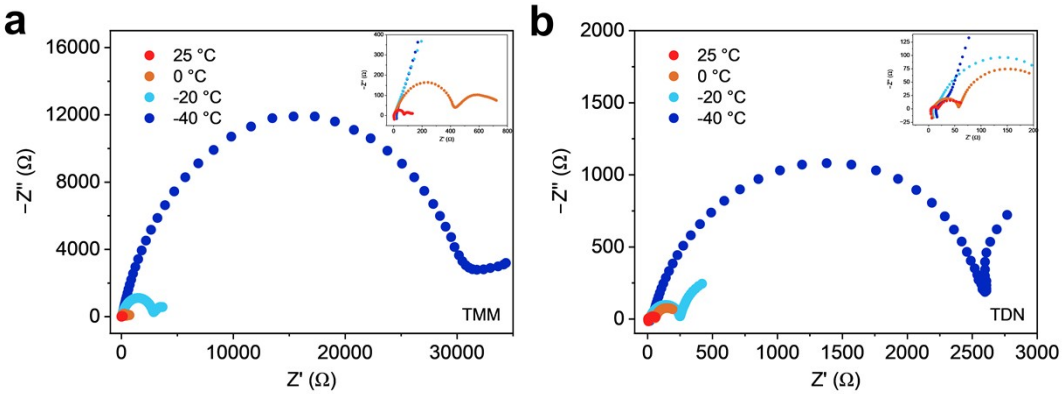

Fig. S11 EIS plots of cycled Li||Li cells at different temperatures (a) TMM and (b) TDN electrolyte.

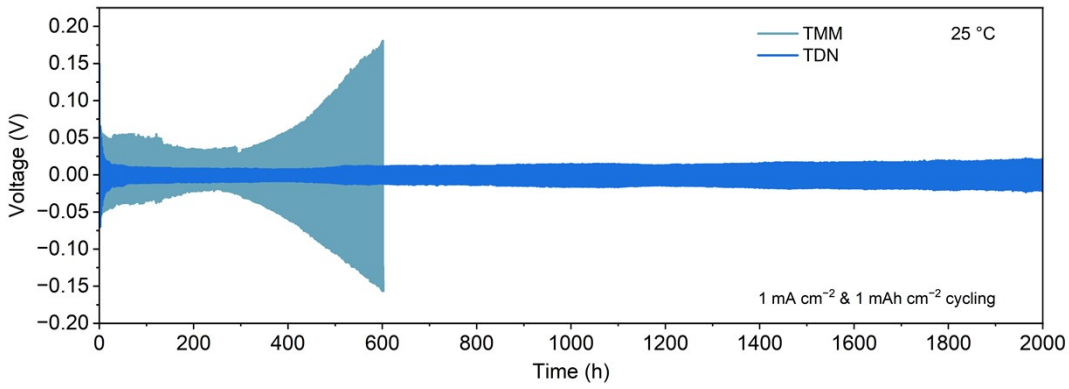

Fig. S12 Long cycling performance of Li||Li cells with different electrolytes at 1 mA cm^{-2} and 1 mAh cm^{-2} at 25 °C.

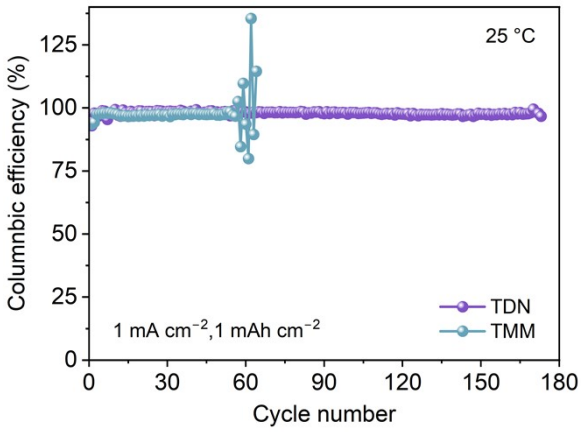

Fig. S13 Li||Cu half cells with the TMM and TDN electrolytes at 1 mA cm^{-2} and 1 mAh cm^{-2} under 25 °C.

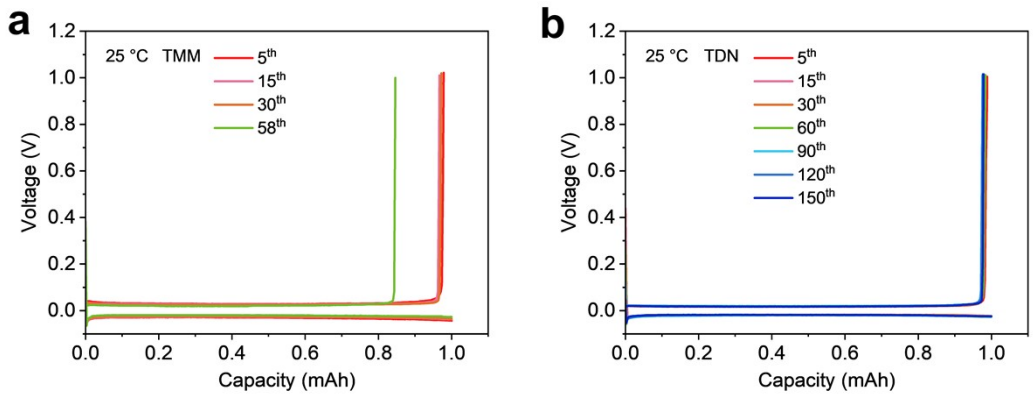

Fig. S14 Capacity-voltage curve corresponding to Figure S12 (a) TMM, (b) TDN electrolyte.

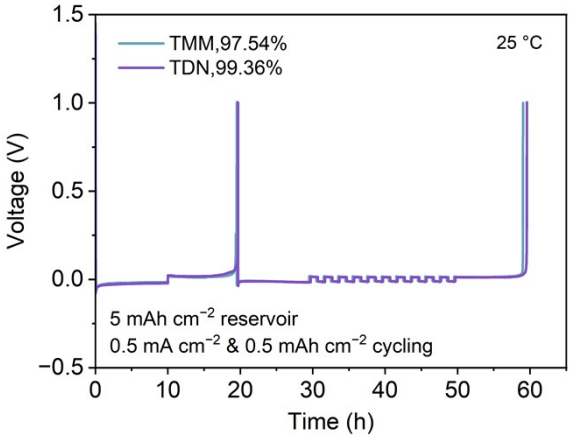

Fig. S15 Aurbach CE in Li||Cu half-cells using different electrolytes under 0.5 mA cm^{-2} at 25 °C.

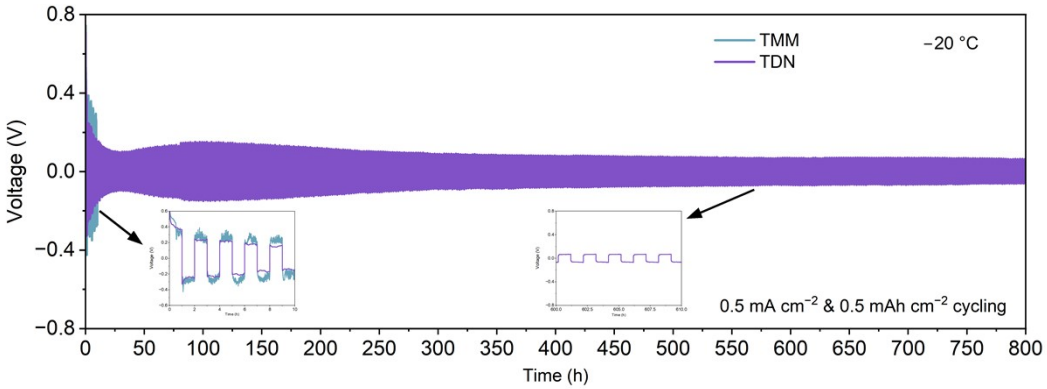

Fig. S16 Long cycling performance of Li||Li cells with different electrolytes at 0.5 mA cm^{-2} and 0.5 mAh cm^{-2} at −20 °C.

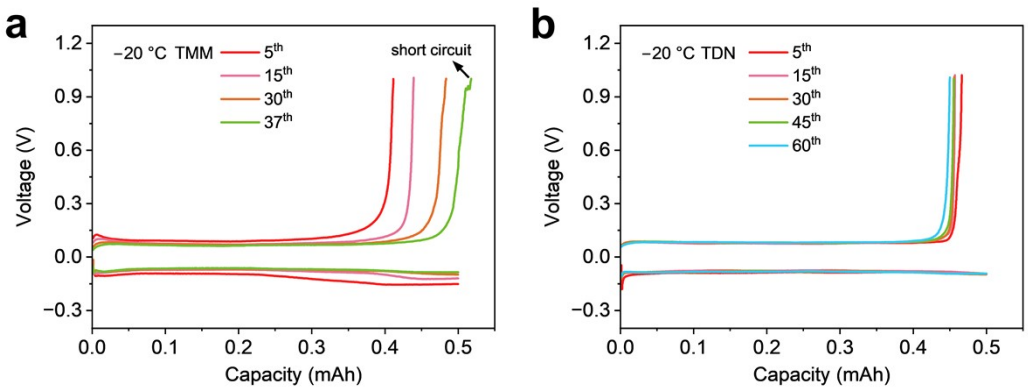

Fig. S17 Capacity-voltage curve corresponding to Figure 4e (a) TMM, (b) TDN electrolyte.

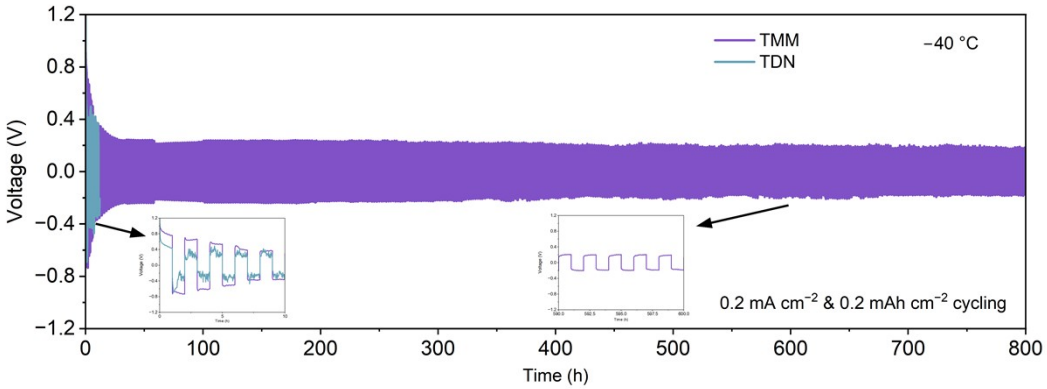

Fig. S18 Long cycling performance of Li||Li cells with different electrolytes at 0.2 mA cm^{-2} and 0.2 mAh cm^{-2} at −40 °C

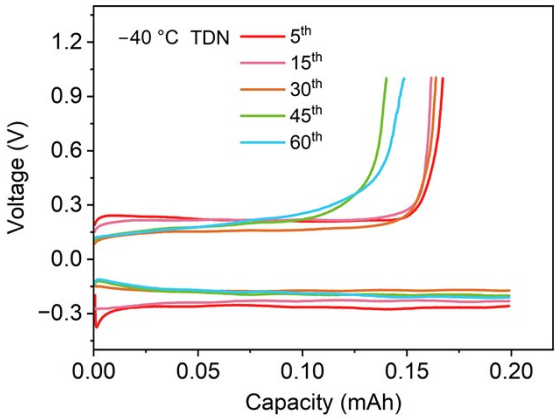

Fig. S19 Capacity-voltage curve corresponding of TDN electrolyte to Figure 4g.

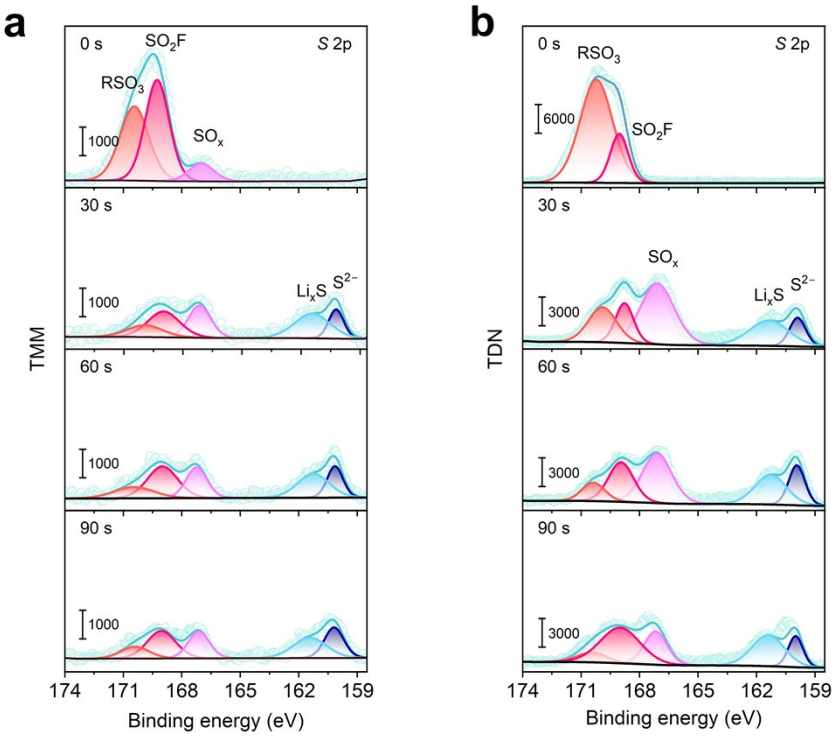

Fig. S20 S 2p regions in XPS spectra of SEI on the Li metal at different sputtering times (0 s, 30 s, 60 s, 90 s) (a) TMM and (b) TDN electrolyte.

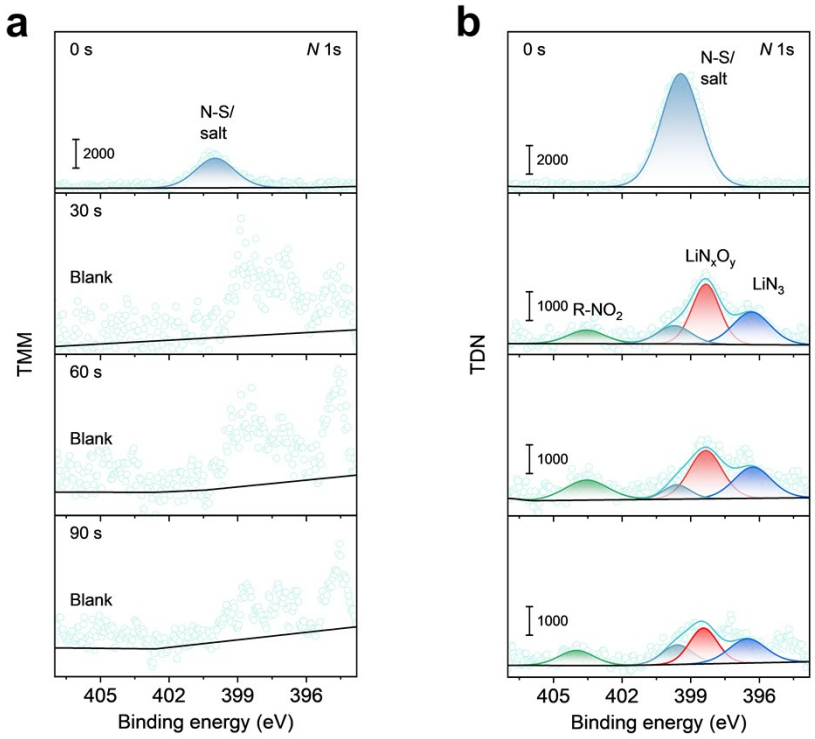

Fig. S21 N 1s regions in XPS spectra of SEI on the Li metal at different sputtering times (0 s, 30 s, 60 s, 90 s) (a) TMM and (b) TDN electrolyte.

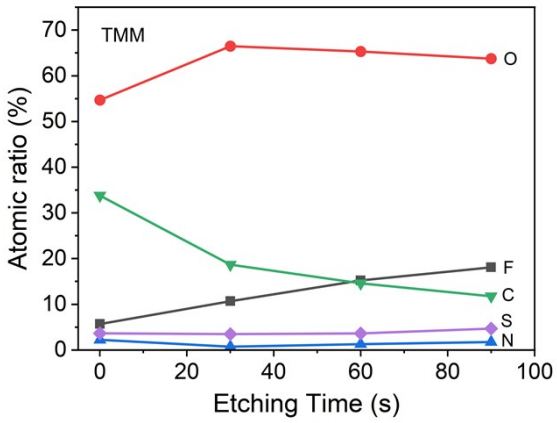

Fig. S22 The atomic percentages at different sputtering time for TMM electrolyte.

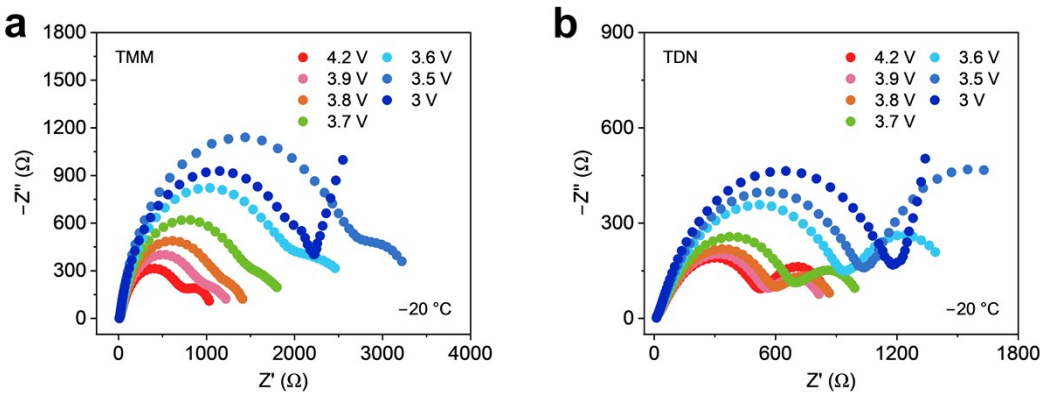

Fig. S23 EIS profiles of the NCM||Li full cells during discharging at −20 °C.

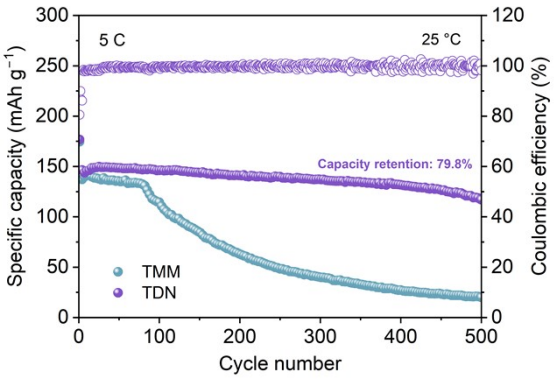

Fig. S24 Cycling performance of Li||NCM811 full-cell with the TMM and TDN electrolytes. at 5 C and 25 °C.

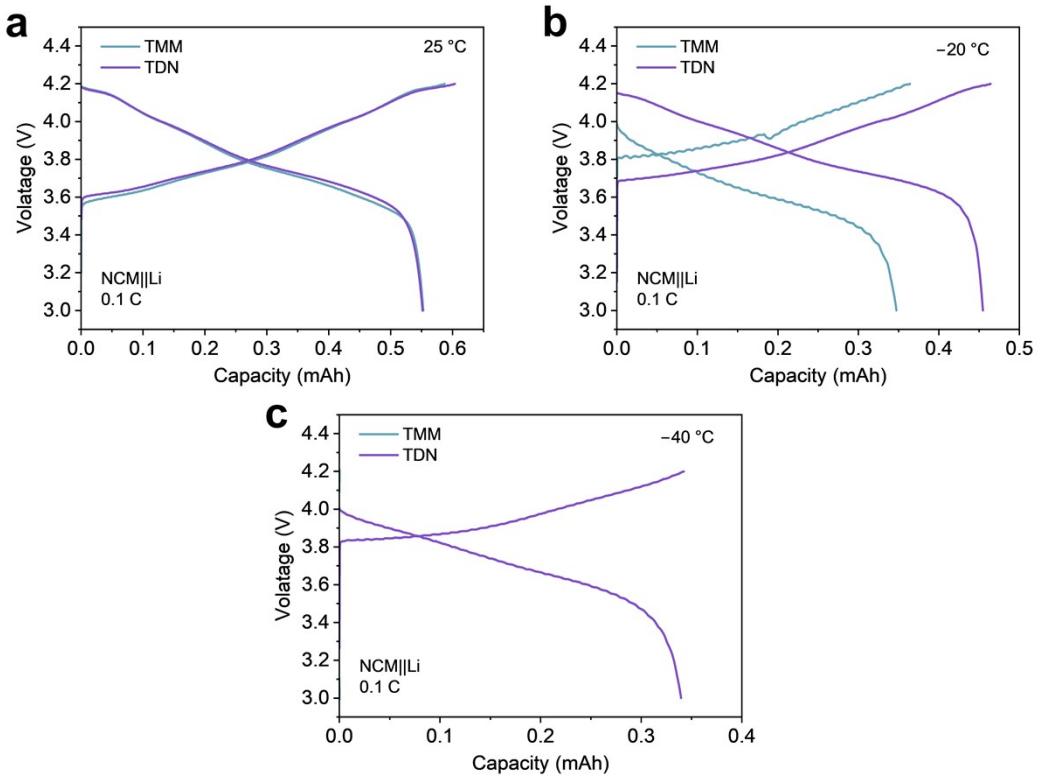

Fig. S25 Capacity-voltage curve corresponding to Figure 5a at different temperatures, (a) 25 °C, (b) −20 °C, and (c) −40 °C.

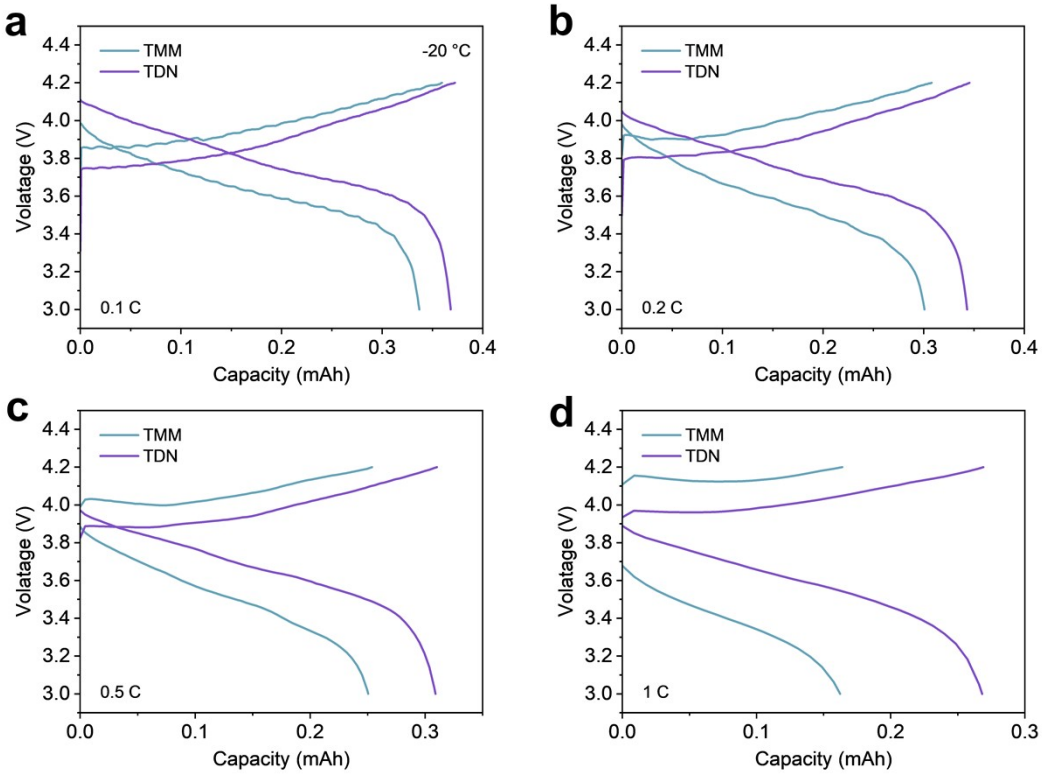

Fig. S26 Capacity-voltage curve corresponding to Figure 5b at different charge-discharge rates, (a) 0.1C, (b) 0.2C, (c) 0.5C, and (d) 1C

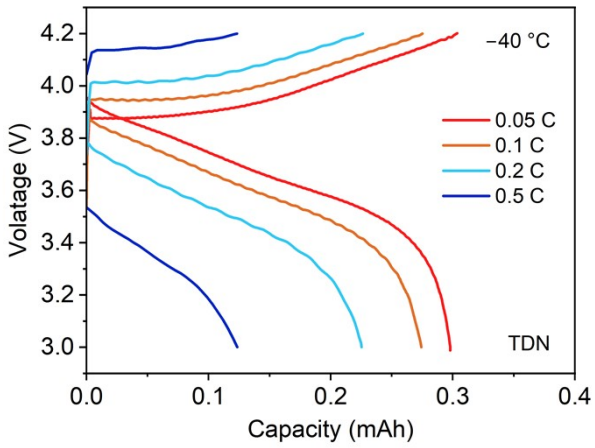

Fig. S27 Capacity-voltage curve corresponding to Figure 5d at different charge-discharge rates with TDN electrolyte

Table 1 Physicochemical properties of various solvents.[8-10]

Solvent	Freezing point (°C)	Bowling point (°C)	Viscosity (mPa s)
DME	-58	85	0.417
TMM	-53	100.6	N/A
DOL	-95	78	0.59

Table 2 Proportion of different solvation structures in TMM and TDN electrolytes at 25 °C.

TMM		**TDN**	
TMM: FSI^-	Percentage (%)	TMM: DOL: FSI^-:NO_3^-	Percentage (%)
3：0	79.64%	3：0：0：0	40.45%
2：1	15.88%	2：0：1：0	18.47%
3：1	1.70%	2：1：0：0	9.60%
2：2	1.64%	2：1：1：0	6.36%
2：0	0.97%	2：0：0：1	5.85%
1：2	0.18%	2：0：2：0	2.10%
		2：2：0：0	2.05%
		1：2：1：0	1.70%
		1：1：2：0	1.42%
		1：1：1：1	1.42%
		1：0：1：2	1.25%
		2：1：0：1	1.14%
		2：0：1：1	1.14%
		1：1：0：2	1.14%
		1：2：0：1	1.02%
		3：0：1：0	0.97%
		2：0：0：0	0.91%
		1：0：2：1	0.51%
		3：1：0：0	0.45%
		1：0：1：1	0.40%
		1：0：0：2	0.34%
		1：0：2：0	0.28%
		2：0：0：2	0.28%
		1：1：1：0	0.23%
		1：1：0：1	0.23%
		3：0：0：1	0.11%
		1：2：0：0	0.06%
		1：0：3：0	0.06%
		1：2：1：1	0.06%

References

1. B. D. Adams, J. Zheng, X. Ren, W. Xu and J.-G. Zhang, Accurate Determination of Coulombic Efficiency for Lithium Metal Anodes and Lithium Metal Batteries, Adv. Energy Mater., 2018, 8, 1702097.
2. T. H. Wan, M. Saccoccio, C. Chen and F. Ciucci, Influence of the Discretization Methods on the Distribution of Relaxation Times Deconvolution: Implementing Radial Basis Functions with DRTtools, Electrochim. Acta, 2015, 184, 483-499.
3. T. Lu and F. Chen, Multiwfn: A multifunctional wavefunction analyzer, J. Comput. Chem., 2012, 33, 580-592.
4. W. Humphrey, A. Dalke and K. Schulten, VMD: Visual molecular dynamics, J. Mol. Graphics, 1996, 14, 33-38.
5. J. Wang, R. M. Wolf, J. W. Caldwell, P. A. Kollman and D. A. Case, Development and testing of a general amber force field, J. Comput. Chem., 2004, 25, 1157-1174.
6. C. I. Bayly, P. Cieplak, W. Cornell and P. A. Kollman, A well-behaved electrostatic potential based method using charge restraints for deriving atomic charges: the RESP model, J. Comput. Chem., 1993, 97, 10269-10280.
7. I. Leontyev and A. Stuchebrukhov, Accounting for electronic polarization in non-polarizable force fields, Phys. Chem. Chem. Phys., 2011, 13, 2613-2626.
8. Y. Yang, Z. Li, M. Zhang, J. Wang, Y. Wang, J. Qiu and H. Zhao, Electrolyte Chemistry Modulation Toward High-Performance and Ultralow-Temperature Silicon Anode, Adv. Mater., 2025, 37, 2417981.
9. H. Zhang, Z. Q. Zeng, F. F. Ma, Q. Wu, X. L. Wang, S. J. Cheng and J. Xie, Cyclopentylmethyl Ether, a Non-Fluorinated, Weakly Solvating and Wide Temperature Solvent for High-Performance Lithium Metal Battery, Angew. Chem., Int. Ed., 2023, 135, e202300771.
10. X. Wang, C. Ji, H. Chen, Y. Liu, Z. Ye, T. Hou and Z. Li, Size-Induced High Entropy Effect for Optimized Electrolyte Design of Lithium-Ion Batteries, Adv. Mater., 2025, 37, e14068.